JOURNAL OF CATALYSIS **170,** 346–356 (1997)
ARTICLE NO. CA971759

Synergetic Effects in the Ni–Mo–O System

Influence of Preparation on Catalytic Performance in the Oxidative Dehydrogenation of Propane

O. Lezla,* E. Bordes,*,[1] P. Courtine,* and G. Hecquet†

*Département de Génie Chimique, Université de Technologie de Compiègne, B.P. 20-529, 60205 Compiègne Cedex, France; and †Elf-Atochem, 4 Cours Michelet, Cedex 42, 92091 Paris-La Défense 10, France

Received April 10, 1995; revised May 16, 1997; accepted May 28, 1997

In the Ni–Mo–O system, the addition of molybdenum oxide to nickel molybdate significantly increases its performance as a catalyst in the oxidative dehydrogenation of propane to propene. The most effective composition is Mo/Ni = 1.27/1, for which a selectivity of 63 mol% in propene is obtained at a propane conversion of 22 mol% (500°C, $\tau = 3.8$ s, $C_3/O_2/H_2O/N_2 = 20/10/30/40$). Several methods of preparation have been used and Mo/Ni ratios were varied from 0.90 to 2.15. Chemical analyses, X-ray diffraction patterns and infrared spectra show that the solid precursor of Mo/Ni > 1 catalysts contains two ammonium salts, $NH_4(NiMoO_4)_2OH \cdot H_2O$ and $(NH_4)_4NiH_6Mo_6O_{24} \cdot 5H_2O$. During calcination, these salts give rise to α-$NiMoO_4$ and to a mixture of α-$NiMoO_4$ and MoO_3 (molar ratio $NiMoO_4/MoO_3 = 1/5$), respectively. DTA/TGA shows that the relative rates of their decomposition during calcination depend on the method of preparation. These experiments permit the precursors to be classified as type I, II, or III materials. The crystallization of MoO_3 proceeds at a lower temperature for type I than for type II material (280 instead of 380°C) and before the crystallization of α-$NiMoO_4$ (ca 450–455°C). No DTA or TGA signal accounts for crystallization of MoO_3 or α-$NiMoO_4$ in type III material. In calcined type I material, the polymorphic transition $\alpha \rightarrow \beta$-$NiMoO_4$ is advanced because of the presence of MoO_3, and MoO_3 itself does not sublime easily. Type I catalysts exhibit better catalytic properties than other types. In differential conditions (500°C, $\tau = 0.2$ s), a synergetic effect is observed with Mo/Ni = 1.27 (type I) catalyst, the conversion of propane being maximum. Coherent interfaces between the (010) plane of α-$NiMoO_4$ and the (100) plane of MoO_3 are shown by transmission electron microscopy. As tentatively explained in the discussion, these interfaces are formed during calcination of type I precursors, the decomposition of which determines the way the reactive microdomains of $NiMoO_4$ are distributed throughout the catalyst in the presence of, and/or onto, crystallites of MoO_3. In turn, the catalytic properties of $NiMoO_4/MoO_3$ (Mo/Ni > 1) are enhanced for the oxidative dehydrogenation of propane to propene.

INTRODUCTION

The selective oxidation and oxidative dehydrogenation of alkanes is a challenging problem because alkanes are less reactive than the obtained products, such as alkenes, dienes or aldehydes, and acids. At the high temperatures which are required to activate alkanes properly, the products can react quickly with cofed oxygen to form combustion products. To overcome this problem, it is necessary to find a catalyst able to activate the C–H bond of the alkane and to provide surface oxygens with suitable energy, just reactive enough to avoid total oxidation. The important operating parameters are the reaction temperature, the alkane to oxygen ratio, and the contact time. As far as propene productivity is concerned, the best catalysts belong to [V–Mg–O] (1–4), [Ni–Mo–O] (5, 6), and [V–Nb–O] systems (7, 8). A comparison between them and others is given by Cavani and Trifirò (9) and a review on the subject appeared recently (10). Using nickel molybdate, Mazzocchia *et al.* (5, 6) found a conversion of 24.8 mol% and selectivity of 37.5 mol% at 560°C and $C_3H_8/O_2/N_2 = 15/15/7$. They claimed that the high temperature form, β, of $NiMoO_4$, is more active and selective than α-$NiMoO_4$. We have carried out catalytic experiments with Mo/Ni > 1 and found that, in this case, the α form of $NiMoO_4$ is the most active and selective. Moreover, we have tried to improve the catalytic properties by arranging for an excess of MoO_3 to be present over that needed to give stoichiometric $NiMoO_4$ after calcination. Several experiments carried out on alkene oxidation (11–22), as well as on butane oxidation (23), have already shown that a molybdenum to metal ratio Mo/M greater than one, or, in other words, the presence of molybdenum oxide beside metallic molybdates, enhances their properties. In the present paper we report on the influence of the preparation method of Ni–Mo–O catalysts on their catalytic performance, and more particularly, on the synergetic effect observed for some of them.

[1] To whom correspondence should be addressed. Fax: +33-3-4423-1980. E-mail: Elisabeth.Bordes@utc.fr.

0021-9517/97 $25.00

EXPERIMENTAL

Several methods of preparation and activation of the precursors [Ni–Mo–O] have been used. The samples are labelled with letters (P for precipitation, ED for evaporation to dryness, etc.), followed by a number (Table 1). Solids obtained after drying in an oven are called "precursors," which, by calcination, yield "catalysts." The solid catalysts were ground to a fine powder and pressed as thin pellets (diameter 2 mm, thickness 0.5 mm), and then activated *in situ* in the catalytic reactor before the catalytic experiments (*vide infra*).

—*Precipitation* (samples P1 to P13) (21). Precursors of various Mo/Ni ratios have been precipitated from a solution of nickel nitrate (Prolabo RP) to which ammonium heptamolybdate (Labosi) was added stepwise. Temperatures of reaction were 85 or 95°C, the pH ranged from 4.4 to 5.6 by addition of HNO_3, and the concentration of nickel was 0.1 or 0.4 M. Thirteen samples were obtained by varying these conditions, four of them having Mo/Ni < 1 (P10–P13). The obtained hot precipitate was filtered, washed with hot distilled water, and dried in an oven at 110°C (12 h). The resulting solid was ground by hand and heated at 320°C during 1.5 h, then ground and heated again at 520°C for 2 h.

—*Evaporation to dryness* (samples ED1-4) (24). Molybdic acid and HNO_3 were added to a solution of nickel nitrate (0.4 *M*) at 80°C. Ammonia was added stepwise up to pH 5. The solution was then evaporated to dryness under stirring. The obtained solid was dried, ground, and calcined as in the method above. Hexagonal and orthorhombic MoO_3 were prepared by decomposition of freshly precipitated ammonium heptamolybdate in a furnace at 250 and 400°C (5 h), respectively. MoO_3 supported on TiO_2 anatase was prepared according to Akimoto and Echigoya (26), by desiccation of a suspension containing an aqueous solution of molybdic and oxalic acids and TiO_2 powder (Thann et Mulhouse, AT1, 7 $m^2\ g^{-1}$) after 3 h stirring, followed by calcination (500°C, 5 h).

—*Sol-gel* (SG) (25). Citric acid (1 mol/Ni) was added to a solution of nickel nitrate (0.4 *M*). A solution of ammonium heptamolybdate was added very slowly so as to avoid precipitation. The solution was evaporated until a gel and then a solid was obtained (28). This solid was then ground and heated in air at 500°C during 24 h.

—*Impregnation* (Imp) (11, 16). The precursor $NH_4(NiMoO_4)_2OH \cdot H_2O$ was first prepared, in a similar manner to the potassium salt of cobalt molybdate $K(CoMoO_4)_2OH \cdot H_2O$ (29, 31). It was precipitated from a solution of ammonium heptamolybdate and nickel nitrate (0.1 *M*)

TABLE 1

Characterization of Mo/Ni ≥ 1/1 Precursors and Catalysts According to the Method of Preparation

Method of preparation	Before calcination: Surf. area (m^2/g)	Before calcination: MoO_3[a] present (wt.%)	Before calcination: Mo/Ni (atomic ratio)	After calcination: MoO_3[a] present (wt.%)	After calcination: Mo/Ni (atomic ratio)	TGA[b] MoO_3 lost (wt.%)	Type[c] of precursor
Precipitation							
P1	26	3.5	1.05	0.2	1.00	1.6	I
P2	24	4.5	1.07	5.0	1.07	1.6	
P3	24	17.5	1.27	18.0	1.27	7.8	
P4	28	22.0	1.33	22.5	1.34	11.0	
P5	21	76.0	2.15	75.8	2.15	3.0	
P6	19	5.5	1.08	6.5	1.10	6.0	II
P7	23	14.0	1.21	15.0	1.22	13.0	
P8	25	17.0	1.26	17.0	1.26	15.0	
P9	18	23.5	1.36	25.5	1.39	27.0	
Evaporation							
ED1	31	2.8	1.04	2.7	1.04	0.5	I
ED2	5	6.1	1.09	n.m	1.09	n.m.	II
ED3	21	13.0	1.20	13.0	1.20	1.0	I
ED4	23	32.5	1.49	32.0	1.49	1.5	I
Sol-gel (SG)	21	5	1.07	2.1	1.03	n.m.	III
Impregnation (Imp)	24	18	1.27	n.m.	—	17.0	III
Mechanical mixture (MM)	20	18	1.27	n.m.	—	20.0	II

[a] Chemical analysis: wt of MoO_3 (g) per 100 g of $NiMoO_4$.
[b] TGA experiments: wt.% lost as MoO_3.
[c] See text; n.m.: not measured.

(Mo/Ni = 1/1) at pH 5.4 and at 85°C. After drying (110°C, 12 h) this solid was impregnated with a solution of ammonium heptamolybdate (0.016 *M*) (Mo/Ni = 1.27/1). The compound was then dried at 110°C and heated in air at 520°C (2 h).

—*Mechanical mixture* (MM) (16). The precursor $NH_4(NiMoO_4)_2OH \cdot H_2O$ prepared as above was mixed with MoO_3 (Mo/Ni = 1.27/1) and the powder was ground by hand in a mortar.

The catalytic experiments were performed at 1 atm pressure in a conventional fixed bed flow reactor with on-line analysis of feed and products by gas chromatography. The stainless steel reactor (10 mm i.d., 565 mm length) containing 4 to 5 g of pelletized catalyst and glass beads was heated by means of an electric furnace regulated to ±1°C. The main part of the effluent leaving the reactor passed through bubblers and was directed to two chromatographs (FID and TCD for hydrocarbons and permanent gases, respectively). At the outlet of the reactor, a diverted portion of the effluent was led to a third chromatograph (FID) for analysis of oxidized products (acrolein, acrylic acid, acetic acid, etc.). General operating conditions were 300–550°C, contact times 1.8–3.8 s (0.69–1.38 $g_{cat.}h \cdot l^{-1}$), feed 20% C_3H_8, 10% O_2, 70% N_2. A low contact time (0.2 s) was used to study the initial catalytic reactivity. Steam was fed by a water pump (20% C_3H_8, 10% O_2, 40% N_2, 30% H_2O), after activation of the catalyst. Blank runs showed no activity of the empty reactor.

Precursors and catalysts before and after catalytic tests were analyzed by elementary chemical analysis, BET method, X-ray diffraction (XRD, Cu Kα), infrared spectroscopy (KBr discs), electron paramagnetic resonance (EPR), and electron microscopy (SEM and HRTEM). Thermal analyses of the behavior of precursors (DTA-TGA) were performed up to 800°C in an air flow ($2\,l \cdot h^{-1}$) at a heating rate of 5°C/min.

RESULTS

1. *Characterization of Solid Precursors and Catalysts*

The specific surface areas of Mo/Ni > 1/1 or <1/1 precursors are in the same range (20–25 $m^2\ g^{-1}$) (Tables 1 and 2) and do not change after catalytic experiments. They are smaller for pure phases (surface area of MoO_3, 1.5; MoO_3/TiO_2, 5.7; α-$NiMoO_4$, 19 $m^2\ g^{-1}$, respectively). The chemical composition of solid precursors (before calcination) and catalysts (after calcination) was determined by chemical analysis. The value of Mo/Ni initially chosen for preparation is roughly the same after calcination (Table 1). The composition is also expressed as the weight of MoO_3 per 100 g of $NiMoO_4$. In the case of P1, the discrepancy between the initial and final Mo/Ni ratios shows that the precursor $NH_4(NiMoO_4)_2OH \cdot H_2O$ was not pure, although it yielded pure $NiMoO_4$ after calcination. From that point of view, the sol-gel method does not seem appropriate to prepare our SG samples. The composition of Mo/Ni < 1/1 samples (P11–P14) is expressed as the weight of NiO per 100 g of $NiMoO_4$ (Table 2). In the XRD pattern of these samples, the lines of NiO are not present but the two forms of $NiMoO_4$, α and β, are found together. The XRD patterns and IR spectra of Mo/Ni > 1 catalysts show that in all cases orthorhombic MoO_3 is present beside α-$NiMoO_4$ (P1–P10, ED1–ED4). In every case the same phases are still present after catalytic experiments, except for pure α-$NiMoO_4$ (Mo/Ni = 1/1) (P1), which is transformed into MoO_2 and NiO. When Mo/Ni > 1 catalysts are heated to 800°C in air (TGA), MoO_3 begins to sublime; some catalysts lose very little weight while others lose more (Table 1). These experiments, together with those related to the thermal behavior of precursors which will be described in the next section, allow the catalysts to be classified into three types, called I, II, and III, respectively (Tables 1 and 2).

TABLE 2

Characterization of Mo/Ni < 1/1 Precursors and Catalysts According to the Method of Preparation

Preparation by precipitation	Before calcination			After calcination		Type[c] of precursor
	Surf. area (m^2/g)	NiO[a] present (wt.%)	Mo/Ni (atomic ratio)	NiO[a] present (wt.%)	Mo/Ni (atomic ratio)	
P10	23	4.0	0.89	3.5	0.90	III
P11	23	2.5	0.93	1.8	0.95	
P12	22	2.5	0.93	1.5	0.96	
P13	19	2.5	0.93	1.5	0.96	

The XRD patterns of the solid precursors prepared by methods P and ED show that two ammonium salts of Ni and Mo are present in variable amounts, according to the initial Mo/Ni ratio and the method of preparation. One is $(NH_4)_4NiH_6Mo_6O_{24} \cdot 5H_2O$, a heteropolyanionic salt (Mo/Ni = 6/1), and the other is a metallomolybdate, $NH_4(NiMoO_4)_2OH \cdot H_2O$ (Mo/Ni = 1). These two salts will hereafter be called HPA and MMo, respectively. Pure HPA (catalyst P5) was prepared with the same raw materials (ammonium heptamolybdate and nickel nitrate) as for MMo, but with different conditions (Ni 0.4 *M*, Mo/Ni = 6/1, 8 h stirring, room temperature). The crystal structure of sodium nickelotungstate hydrate having been already solved by Eriks *et al.* (29), we have indexed the XRD powder pattern of the structurally similar Mo-containing HPA and proposed the cell parameters accordingly (Table 3). The infrared spectrum of HPA (Fig. 1b) agrees well with the one presented by Nomiya *et al.* (29). Indexation of the XRD pattern of $NH_4(NiMoO_4)_2OH \cdot H_2O$ (MMo, catalyst P1) has been made on the basis of its isotypy with other metallomolybdates such as $K(CoMoO_4)_2OH \cdot H_2O$ (30, 31) (Table 4). As

TABLE 3

Indexation of the XRD Pattern of Precursor $(NH_4)_4NiH_6Mo_6O_{24} \cdot 5H_2O$ (HPA)

d_{obs} (Å)	d_{calc}[a] (Å)	I/I_0	hkl
10.8	10.8	37	010
7.9	7.9	51	100
7.2	7.1	19	001
5.82	5.79	46	101
5.40	5.39	30	020
5.05	5.05	80	111
3.74	3.73	35	201
3.12	3.12	42	031
3.02	3.01	100	211
2.77	2.78	24	212
2.71	2.70	33	040
2.62	2.62	22	032
2.55	2.56	11	122
2.499	2.494	20	310
2.425	2.422	16	141
2.356	2.352	8	311
2.316	2.316	18	113
2.280	2.281	11	313
2.246	2.246	17	330
2.230	2.229	21.5	232
2.068	2.066	11	321
1.866	1.867	20.5	331
1.793	1.7933	15	133
1.734	1.7360	12	351
1.710	1.7106	15.5	214
	1.7103		252

Note. Space group: $P\bar{1}$; Triclinic. Cell parameters: a = 8.05 Å; b = 10.86 Å; c = 7.25 Å; $\alpha = 93.02°$; $\beta = 99.01°$; $\gamma = 95.73°$. Density: $d_{calc} = 2.26$ g cm^{-3}; $d_{obs} = 2.36$ g cm^{-3}.

[a] Calculated.

TABLE 4

Indexation of the XRD Pattern of Precursor $NH_4(NiMoO_4)_2OH \cdot H_2O$ (MMo)

d_{obs} (Å)	d_{calc}[a] (Å)	I/I_0	hkl
8.2	8.2	25	001
5.0	4.9	14	111
4.30	4.33	20	200
4.11	4.08	26	002
3.35	3.33	37	201
3.28	3.26	100	020
3.02	3.03	85	021
2.814	2.826	24	311
2.700	2.705	20	312
	2.700		113
2.479	2.479	20	22-2
2.219	2.213	15	113
2.064	2.055	18	004
1.910	1.914	16	404
1.737	1.722	25	330

Note. Possible space groups: $C_{2/m}$, C^3_{2h}. Density: $d_{calc} = 3.156$ g cm^{-3}; $d_{obs} = 3.26$ g cm^{-3}.

[a] Calculated.

expected, the IR spectra of $NH_4(NiMoO_4)_2OH \cdot H_2O$ and $K(CoMoO_4)_2OH \cdot H_2O$ (32) are closely related, except for bands near 1400 cm^{-1} which are assigned to NH_4^+ (Fig. 1a).

EPR experiments were performed on some samples in order to detect the presence of Mo^{5+} species after the catalytic test. For example, the spectrum of P2 (type I) at room temperature is characteristic of the presence of Mo^{5+}. However, the signal is broad and isotropic as in the case of interactions between nonisolated Mo^{5+} species ($g_{iso} = 1.519$) (33). TEM experiments on types I and II after calcination show the presence of MoO_3 and of α-$NiMoO_4$ which were characterized by their microdiffraction pattern. Particles of α-$NiMoO_4$ can be superimposed on crystals of MoO_3. In the case of a type I sample, a high resolution electron micrograph at magnification 4,000,000 (Fig. 2) shows that a (010) face of α-$NiMoO_4$ ($d_{020} = 4.37$ Å) covers a (100) face of MoO_3 ($d_{200} = 1.98$ Å).

2. *Study of the Reactivity of Precursors and Catalysts*

As just described, the methods of characterization show that all methods of preparation of Mo/Ni > 1 samples (except MM) yield solids containing both HPA and MMo. Both α-$NiMoO_4$ and MoO_3 are found in the XRD patterns of the corresponding Mo/Ni > 1 catalysts. Apart from the fact that the amount of MoO_3 is different, it is not easy to understand why some catalysts exhibit better catalytic properties than others, as will be seen in the next section. Since the history of the sample is very determinant for its catalytic properties, we have examined the behavior of the precursors by DTA/TGA in air (Table 5). For each sample, the heating has been stopped just after endo- or exothermic peaks and XRD on the quenched solid has been performed to identify the phase(s) present at this stage of transformation. The decomposition of pure HPA (Mo/Ni = 6/1) and of pure MMo (Mo/Ni = 1/1) was first studied. Several features

TABLE 5

Temperature (°C) of DTA Peaks Observed During the Heating in Air of Pure HPA, Pure MMo, and of Precursors (Mo/Ni ≥ 1/1)

Precursor	Endotherms[a]	Exotherm[b]	Exotherm[c]
HPA (Mo/Ni = 6/1)	90, 165, 225, 270	380	450
MMo (Mo/Ni = 1/1)	60, 150, 220	—	455
Type I	130, 180	280[d]	450–500[e]
Type II	60, 165, 230	380	450–500[e]
Type III	80, 150, 225–390	—	—

[a] Endotherms attributed to loss of H_2O and NH_3.

[b] Ascribed to crystallization of MoO_3.

[c] Ascribed to crystallization of α-$NiMoO_4$.

[d] Simultaneous decomposition (exo) of NH_4NO_3 and crystallization (endo) of MoO_3.

[e] Mean range for various samples.

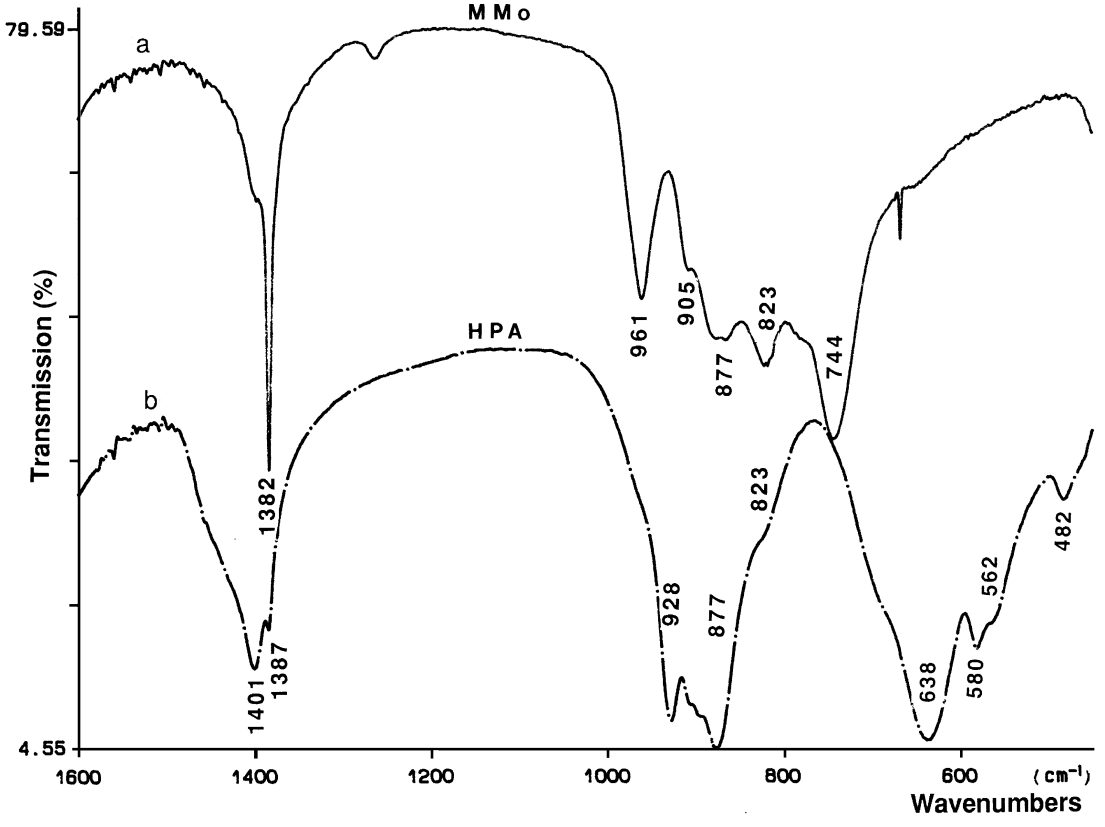

FIG. 1. Infrared spectra (1700–400 cm^{-1}) of (a) $NH_4(NiMoO_4)_2OH \cdot H_2O$ (MMo) and (b) $(NH_4)_4NiH_6Mo_6O_{24} \cdot 5H_2O$ (HPA).

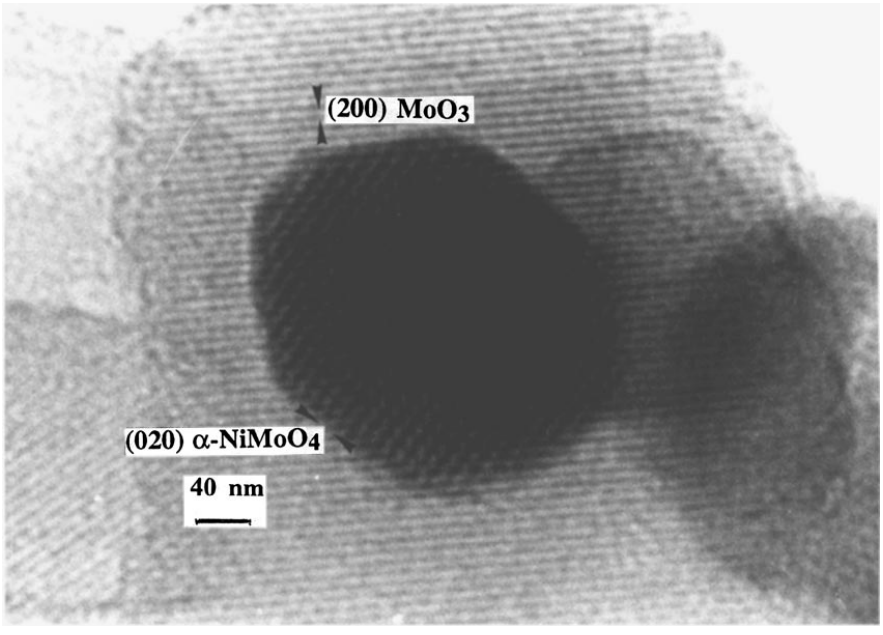

FIG. 2. HRTEM micrograph of α-$NiMoO_4$-MoO_3 (P3) showing the structural adaptation of lattice planes between (010) α-$NiMoO_4$ and (100) MoO_3.

are common: (i), first a loss of weight (several substeps) for endothermal losses of H_2O and NH_3 at 60–280°C, and (ii) an exothermic peak for crystallization of α-$NiMoO_4$ at 450–455°C (Table 5). MMo loses weight up to 455°C and α-$NiMoO_4$ is present at the end of experiments as shown by its XRD pattern. In the case of HPA, the weight is stable above 380°C. A supplementary exothermic peak occurs at 380°C, which is due to the crystallization of MoO_3 as shown by XRD when the solid is quenched after this peak. At the end of experiments, both α-$NiMoO_4$ and MoO_3 are present. Mo/Ni > 1 precursors containing HPA and MMo were studied in a similar way. According to the occurrence (or not) of these signals and their temperature range, the precursors can be classified into the three types already mentioned (Tables 1, 2, and 5). For all precursors, H_2O and NH_3 are lost in the range 60–260°C (types I and II), and up to 390°C for type III. The crystallization of α-$NiMoO_4$ occurs at 450–500°C (types I and II), but no DTA signal accounts for it for type III. The main difference between types I and II is the temperature of crystallization of MoO_3: the exothermic signal, which was observed at 380°C with type II and with HPA, is more intense, very sharp, and observed at lower temperature (280°C) with type I. Traces of ammonium nitrate were observed, together with crystalline MoO_3, in the XRD pattern of solids quenched after this peak. Therefore, we assume that the early crystallization of MoO_3 is associated with the decomposition of some ammonium nitrate present in the samples (34–36). A similar phenomenon was observed during the calcination (followed by DTA/TGA) of $AgFeP_2O_7$ and $CsFeP_2O_7$, prepared with metallic nitrate salts and ammonium phosphates (37). $CsFeP_2O_7$ was shown to act as an active support of Fe–P–O catalysts for the oxidative dehydrogenation of isobutyric acid to methacrylic acid (38).

Another way to differentiate Mo/Ni > 1 catalysts is to heat the precursor at temperatures above 700°C under air flow in a TG apparatus. The weight loss observed (or not) in these conditions is assigned to the sublimation of MoO_3 which begins at various temperatures according to the type of precursor (Table 1): it begins at ca 750–760°C for type II and HPA, but at ca 800°C for most of type I precursors. All of MoO_3 (beside $NiMoO_4$) is lost by type II (as checked by XRD on P6–P9, DE2, MM, Imp), but very little is lost by type I samples. MoO_3 is therefore thought to be stabilized in the presence of α-$NiMoO_4$ in the latter case. Finally, the DTA of the direct and reverse polymorphic transition $\alpha \leftrightarrow \beta$-$NiMoO_4$ was performed. While the endotherm at 720°C ($\alpha \rightarrow \beta$) and exotherm at 290°C ($\beta \rightarrow \alpha$) are observed for $NiMoO_4$ alone (P1, Mo/Ni = 1), as in Ref. (39), these temperatures are lowered for type I (Mo/Ni > 1) catalysts: the transitions proceed at 600 and 185°C, respectively. In other words, the presence of MoO_3 beside $NiMoO_4$ is responsible for the easier transformation of α-$NiMoO_4$ to β-$NiMoO_4$ (by increasing temperature), and the range of thermal stability of β-$NiMoO_4$ is therefore increased.

3. *Catalytic Properties*

The catalytic properties of some pure phases (MoO_3, α-$NiMoO_4$, and β-$NiMoO_4$), and of supported phases (MoO_3/TiO_2-anatase, α-$NiMoO_4$/13% MoO_3, and β-$NiMoO_4$/13% MoO_3) have been compared at $\tau = 1.8$ s (0.69 $g_{cat.} l^{-1} \cdot h$), C_3/O_2/N_2 = 10/10/80 (C_3/O_2 = 1/1), and 350–550°C (Table 6). Orthorhombic MoO_3 is less active but more selective than the hexagonal form. When supported on TiO_2-anatase, the conversion (C) of propane by orthorhombic MoO_3 is greater and the selectivity to propene (S) increases. This is still true at 500°C on a per unit surface area basis, but not at higher temperature (530–550°C). Nickel molybdate alone is more active than MoO_3 since C = 2.5 mol% at 460°C and 40 mol% at 500°C, but at this temperature only products of cracking are observed. Per unit area, the conversions obtained with $NiMoO_4$ at 460°C ($C = 0.18$ mol% $\cdot m^{-2}$) and MoO_3/TiO_2 at 500°C ($C = 0.15$ mol% $\cdot m^{-2}$) are similar, but the former catalyst is slightly less selective. When both α-$NiMoO_4$ and MoO_3 are present (e.g., ED3, 13% MoO_3, Mo/Ni = 1.2/1), the selectivity to propene reaches a high value (S = 72–73 mol%) at moderate conversion. By comparison, β-$NiMoO_4$/13%MoO_3 is less selective and propane conversion is 14 times less at ca 550°C. It must be recalled that, to obtain this β form, the same composition

TABLE 6

Conversion of Propane and Selectivity to Propene for Some Pure and Supported Phases

Catalyst	S.A. (m^2/g)	Temp. (°C)	C_3 Conv. (mol%)	C_3 Conv.[a] (mol% $\cdot m^{-2}$)	Selectivities (mol%) C_3H_6	P.M.O.[b]	CO_x[c]
MoO_3 (orth.)	1.2	500	0.1	0.08	49	2.5	48
		530	0.7	0.58	55	2.0	42[c]
MoO_3 (hex.)	2.0	355	0.2	0.10	19	—	81
		500	1.0	0.50	33	—	67
MoO_3/TiO_2	6.0	470	0.5	0.07	54	—	46
		500	0.9	0.15	55	2.0	42
		550	2.5	0.42	62	2.5	29[d]
α-$NiMoO_4$	19	460	2.5	0.18	52	—	48
α-$NiMoO_4$/ MoO_3[e]	21	500	4.0	0.19	73	6.5	20
		540	7.0	0.33	72	6.5	21
β-$NiMoO_4$/ MoO_3[e]	n.a.	550	0.5	n.a.	61	4.0	34

Note. $C_3/O_2/N_2$ = 10/10/80, $\tau = 1.8$ s (0.69 $g_{cat.} l^{-1} \cdot h$); n.a. = not applicable.

[a] Conversion per unit surface area.
[b] Products of mild oxidation.
[c] $CO + CO_2$.
[d] $+CH_4$, C_2H_4.
[e] 13 wt.% of MoO_3.

ED3 was heated in the reactor to 720°C and then cooled *in situ* to 300°C to avoid the $\beta \rightarrow \alpha$ transition. Catalytic tests were run thereafter. The surface area of the resulting β-$NiMoO_4$/13%MoO_3 catalyst could have been strongly decreased by this thermal treatment, explaining thereby the lower conversion of propane.

The influence of the C_3/O_2 ratio and of steam has been studied using Mo/Ni > 1 catalysts, in conditions allowing propane to be converted while maintaining a good selectivity to propene. For example, using ED3 (type I) with $\tau = 3.8$ s (1.4 $g_{cat.} l^{-1} \cdot h$) at 530°C, the conversion and selectivity increase when the C_3/O_2 ratio is doubled; thus, C = 12 and 13.5 mol%, S = 62 and 72 mol% when $C_3/O_2 = 1/1$ and 2/1, respectively ($C_3/O_2/N_2 = 10/10/80$ and $C_3/O_2/N_2 = 20/10/70$). When steam is added to the feed (30%), the conversion increases up to a mean value (C = 21 mol%) but selectivity decreases to 50 and 65 mol% for $C_3/O_2 = 1/1$ and 2/1, respectively. These values remained the same over 48 h on stream. Steam is thought to avoid coking which is known to affect α-$NiMoO_4$ (40), which we observed, too (34, 35). Therefore, the other catalysts have been studied with a feed containing steam and $C_3/O_2 = 2/1$ ($C_3/O_2/H_2O/N_2 = 20/10/30/40$). In these conditions and at $\tau = 1.8$ s and 500°C, a typical behavior of Mo/Ni > 1 catalysts is shown by P3 (type I) (Fig. 3). The selectivity to propene is the highest at low conversion; this seems to be a characteristic of the selective oxidation of light alkanes (9), including that of ethane to acetic acid (41, 42). The selectivity to propene decreases to 63.5 mol% when the conversion of propane is increased to 22 mol%, owing to the formation of CO_x (S = 32 mol%). The maximum yield of propene is 19.5 mol%. The formation of acrolein passes through a maximum, $S_{acro} = 5.5$ mol% at C = 7 mol%. Very low amounts of ethylene and methane (S < 1 mol%) are found.

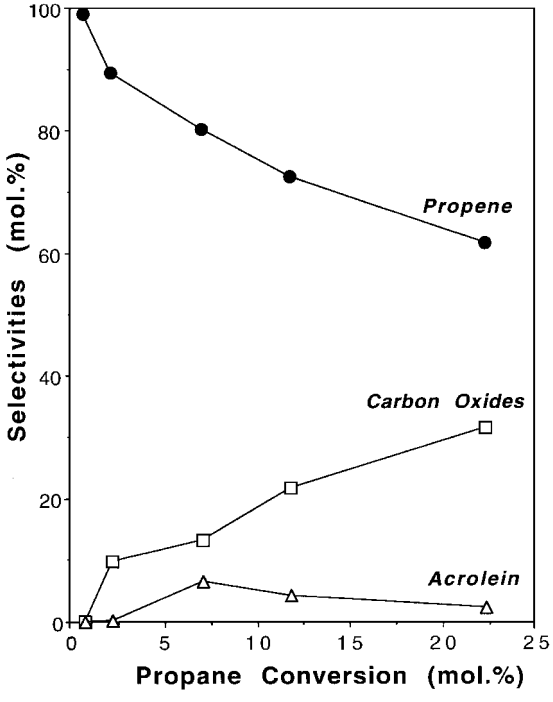

FIG. 3. Selectivities to propene, CO_x and acrolein vs conversion of propane for catalyst P3 (type I) (500°C, $\tau = 1.8$ s, $C_3/O_2/H_2O/N_2 = 20/10/30/40$).

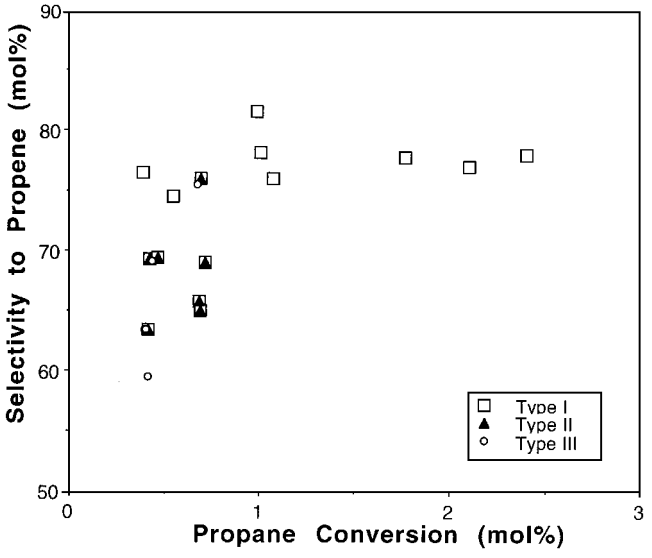

FIG. 4. Selectivity to propene vs conversion of propane (500°C, $\tau = 0.2$ s, $C_3/O_2/H_2O/N_2 = 20/10/30/40$). Influence of the type of solid precursor I, II, and III (see text). Symbols: open squares, type I; filled triangles, type II; open circles, type III.

The influence of preparation according to the type of precursor (and composition) has been studied in the following conditions (differential reactor): 500°C, contact time $\tau = 0.2$ s, total flow rate 5.4 $l \cdot h^{-1}$, 0.317 g_{cat}. The steady state was considered to be reached after 15 h at 500°C. The surface areas being all in the same range (20–25 $m^2\ g^{-1}$), we assume, to a first approximation, that the values of conversion can be directly compared. Figure 4 and Table 7 show that, in the same operating conditions, the best conversions of propane and selectivities to propene are obtained with type I solids. For example, at C = 0.4 mol%, selectivities are 60–63, 63–69, and 76 mol% for types III, II, I, respectively (Fig. 4). Considering the variation of Mo/Ni ratio within type I series, the conversion can be increased up to 2.4 mol%, while in the other cases (types II and III) the increase of conversion is correlated with a strong decrease of selectivity due to the formation of CO_x. At constant Mo/Ni composition (e.g. 18 and 5 wt.%MoO_3), the catalysts prepared by methods P (precipitation) or ED (evaporation to dryness) are very selective and are also the most stable on stream (Table 7). Within catalysts prepared by the same

TABLE 7

Influence of the Method of Preparation and Types I, II, III on the Catalytic Performance for Two Compositions, 18 and 5 wt.% MoO_3

Method	S.A.[a] m^2/g	Type	Conv. mol%	Selectivities (mol%) Propene	Acrolein	CO, CO_2
18 *wt.% MoO_3*						
P3	24	I	2.40	77.9	3.3	18.0
MM	20	II	0.69	65.0	2.0	33.0
Impregn.	24	III	0.71	69.0	2.3	28.7
5 *wt.% MoO_3*						
P2	24	I	1.07	76.0	2.3	20.7
ED1	31	I	0.98	81.6	1.1	16.1
SG	21	III	0.41	59.5	1.8	36.4

Note. $C_3/O_2/H_2O/N_2 = 20/10/30/40$, 500°C, $\tau = 0.2$ s, 0.317 g_{cat}.
[a] after calcination; similar after test ($\Delta SA/SA = 5\%$).

method, type II catalysts exhibit poorer performance (ED2 for evaporation to dryness, P6–P9 for precipitation series). Finally, a synergetic effect is observed when the conversion of propane is plotted against composition in the type I series, while selectivity remains nearly constant (Fig. 5). In the same conditions, the best yield of propene is obtained with P3 (Mo/Ni = 1.27/1) which contains 18 wt.% MoO_3. The catalysts corresponding to pure precursors MMo (P1, type 1) or HPA (P5, type II) are poorly active in these conditions (C = 0.54 and 0.38 mol%, respectively). Obviously, the conversions are low because of differential conditions, but the observed trends are maintained at higher contact times.

DISCUSSION

1. *Influence of Preparation and of the Presence of MoO_3 beside $NiMoO_4$ on Catalytic Properties*

As already observed with other metal molybdates (M = Mn, Co, Fe, U) for other reactions (11–23), our results show that, when MoO_3 is present beside α-$NiMoO_4$ (Mo/Ni > 1), an improvement of the catalytic activity (conversion of propane) and, to a less extent, of the selectivity to propene, results. A synergetic effect is evidenced (Fig. 5) and, moreover, these catalysts are also more stable on stream. Indeed, the irreversible reduction on stream of pure α-$NiMoO_4$ to MoO_2 and NiO observed for higher contact times is inhibited when MoO_3 is present. The presence of β-$NiMoO_4$ or of NiO beside α-$NiMoO_4$ does not seem to produce such a positive effect as MoO_3.

However, the good influence of MoO_3 on the catalytic performance and stability of α-$NiMoO_4$ (Mo/Ni > 1) is observed only when the preparation is made in the "right" way. We have shown that the same constituents, MMo and HPA, are present in all precursors, but that their mixtures exhibit different thermal behaviors allowing a classification of the catalysts (I, II, or III). Higher yields of propene are obtained with catalysts prepared by precipitation (P) or evaporation to dryness (ED), than by impregnation of MMo by molybdate salt (Imp) or mechanical mixture of MMo and MoO_3 (MM). One could expect that HPA alone (type II), which leads to MoO_3 and α-$NiMoO_4$ by calcination, would be a very good catalyst but this is not the case, although it is fairly stable on stream. This means that the relative rates of decomposition of HPA and MMo in the HPA/MMo

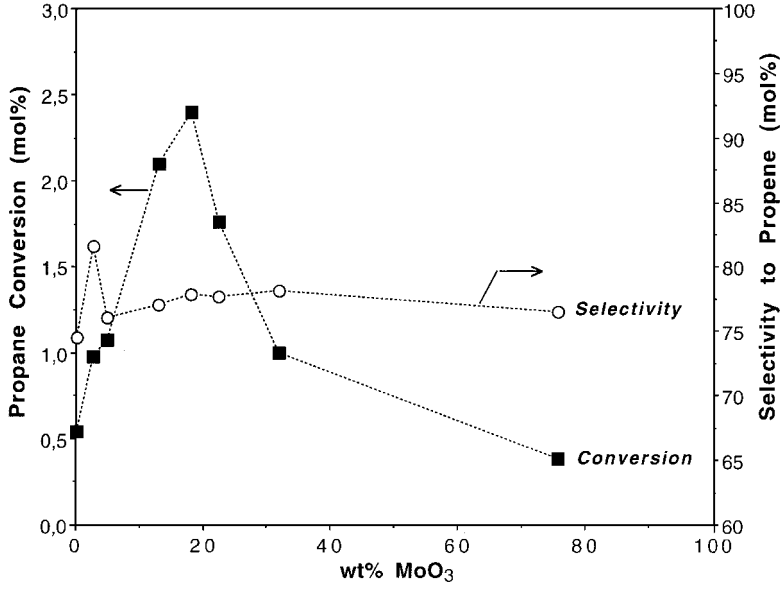

FIG. 5. Conversion of propane and selectivity to propene vs wt.% MoO_3 for type I catalysts (500°C, $\tau = 0.2$ s, $C_3/O_2/H_2O/N_2 = 20/10/30/40$). Symbols: squares, conversion of propane; circles, selectivity to propene.

mixture are determinant in optimizing the kind and number of interactions between particles of MoO_3 and particles of α-$NiMoO_4$. DTA has shown that the crystallization of MoO_3 in type I happens at a temperature far lower (100°C) than in type II and is not detected with type III samples. Without ignoring the fact that heat and mass transfer limitations are probably very different during calcination and during DTA, let us assume that the thermal history of the precursor is similar to a first approximation (same heating rate and atmosphere). For types I and II, $NiMoO_4$ crystallizes at 450–455°C in the presence of the already formed MoO_3 crystallites. However, for type I, there is more "time" for the nuclei of $NiMoO_4$ to develop while interacting with MoO_3 (175°C range) than for type II (75°C range). Another point is that MoO_3 crystallites are smaller when formed at 280°C (broadening of XRD lines), and then more reactive. Whatever the actual phenomenon is, the interactions between MoO_3 and α-$NiMoO_4$ are very strong in type I catalysts. HRTEM pictures like that presented in Fig. 2 are representative of this phenomenon. A strong anchoring between α-$NiMoO_4$ and MoO_3 leading to the stabilization of the latter is in accordance with the hindered sublimation, even at high temperature, of MoO_3 (Table 1). On the other hand, the easier transformation of α to β-$NiMoO_4$ could be justified also by strong interactions, MoO_3 acting as a "catalyst" of the transition. A similar phenomenon has been observed already, e.g., when the rate of the oxidation of Mn_2O_3 to Mn_3O_4 was increased because of the presence of $MnMoO_4$ (43).

In a former work dealing with multicomponent molybdates active in the (amm)oxidation of propene, we had similarly emphasized the importance of preparation of the precursors (44). Indeed, the way in which the phosphorus and silica are added for optimization of industrial catalysts $M_{11-x}Fe_xBiMo_{12}P_yO_z$, $nSiO_2$ (M^{2+} = Co, Ni, Mn, Mg, $0 < x < 4$) (45) has been found to be responsible for different morphologies. While the usual method (evaporation to dryness of metallic nitrates and molybdate salts) was supposed to be responsible for building successive layers of active molybdates as in the cherry-like model (24), we have shown that the coprecipitation method leads first to the formation of two heteropolysalts, $(NH_4)_3PMo_{12}O_{40} \cdot 4H_2O$ and $(NH_4)_3HSiMo_{12}O_{40} \cdot 5H_2O$ (44). During the decomposition of these heteropolysalts in the presence of metallic salts (calcination), the molybdenum cations were assumed to be distributed among M, Fe, Bi, salts, optimizing thereby the interfacial effects between the final metallic molybdates (46). Ponceblanc *et al.* have demonstrated by several methods that indeed these molybdates are closely interacting (47).

2. *Interfacial Effects between MoO_3 and α-$NiMoO_4$*

Synergetic effects in mild oxidation catalysis have been observed in several cases between an active phase and its support (e.g., V_2O_5/TiO_2) (48), or between two (or more) active phases. Such effects are not restricted to catalysis but are observed also in solid–solid transformations in an inert atmosphere. We have already given several examples of modification of the temperature of, e.g., an allotropic transition (23, 43, 48–50). The common, and necessary condition, established (48) and verified on various examples (23, 46–51), is that the interfaces between the two crystalline phases in contact are coherent. Supported monolayers are not concerned here, although synergetic effects are well known in that case also (52), because the notion of coherent boundaries applies only for crystalline partners. When the crystallographic lattice misfit is small, the surface energy barriers are so lowered that the transfer of electrons and of other larger species like oxygen ions, is easier across the interface. This is the only way to account for the participation of a coredox modifying the active redox couple in mixed oxides (e.g., Mo^{6+}/Mo^{5+} with V^{5+}/V^{4+} in V_2O_5–MoO_3) (41), thereby explaining why the mixed oxide shows better catalytic performance that the single one. The crystallographic mismatches (48) have been computed for several planes of MoO_3 and α-$NiMoO_4$ (Table 8) by using their cell parameters, as in other cases (22, 23, 46–51). The very low values are in accordance with the above hypotheses and account for the interfacial coherence.

Most of the phases (which are selective catalysts of oxidation) able to settle coherent interfaces belong, or are related to, two structural families roughly defined as ReO_3-like oxides and $M_m(M'O_4)_n$ oxysalts. On both sides of the coherent boundaries, the active ions are strained as compared to those in the bulk (46). When no reactive gas is present, the excess energy due to strains is released by mechanical relaxation, which results in the formation of extended defects and/or crystallographic shear planes as proposed by Wadsley in the cases of pure MoO_3 or V_2O_5 and reported by others (53, 54). Depending on the relative metastability of the partners, another result can be the formation of a polymorph, as when TiO_2 anatase is transformed to rutile in the presence of V_2O_5 (48), or when $\alpha \rightarrow \beta$-$CoMoO_4$ in $CoMoO_4$–MoO_3/TiO_2 catalysts

TABLE 8

Cell Parameters and Crystallographic Misfits between the (020) Plane of α-$NiMoO_4$ and the (200) Plane of MoO_3

Parameters[a]	Crystallographic misfit (%)[b]
$c(\alpha\text{-}NiMoO_4)/2c(MoO_3)$	3.5
$2c(\alpha\text{-}NiMoO_4)/b(MoO_3)$	9.6
$c(\alpha\text{-}NiMoO_4)/2a(MoO_3)$	3.3

[a] α-$NiMoO_4$: C^3_{2h} (C2/m), a = 9.509 Å, b = 8.759 Å, c = 7.667 Å; MoO_3: C^3_{2h} (Pbnm), a = 3.962 Å, b = 13.858 Å, c = 3.697 Å.

[b] Crystallographic misfit × 100 = (e.g.) $[c(\alpha\text{-}NiMoO_4) - 2c(MoO_3)]/c(\alpha\text{-}NiMoO_4)$.

(23, 49). Otherwise, the relaxation can be directed toward the chemisorbed gas molecules, instead of being mechanically compensated, leading to catalytic activity. The concept of coherent interfaces is also valid when microdomains (and not only extended defects) of one phase inside another are formed (41). The presence of two phases, e.g. ¯-$VOPO_4$ and $(VO)_2P_2O_7$ during mild oxidation of 1-butene to maleic anhydride, has been found necessary by considering the existence of such coherent boundaries (51).

Consequently, the improved catalytic performance of Mo/Ni > 1 catalysts is related to the necessary presence of both MoO_3 and ®-$NiMoO_4$ and corresponds to one more example of solidÐsolid interfacial effects. As usually observed, there is an optimum range of composition (here ca 18 wt.% MoO_3 in differential conditions), corresponding to the highest conversion of propane and yield to propene. The solidÐsolid transformations observed during decomposition of precursors constitute an additional, although indirect, proof (49), since the crystallization of MoO_3 occurs at a lower temperature (280±C) than usual in type I solids and that the transition ®! ¯-$NiMoO_4$ is advanced at 600°C in the presence of MoO_3 (instead of 720±C for pure $NiMoO_4$ (39). The Tammann temperature of $NiMoO_4$ is therefore decreased, which could be related to higher reactivity.

Another question is to what extent the experimental conditions during preparation are more or less favorable to the formation of microdomains with coherent boundaries. A careful examination of MMo and HPA structures provides some answers (36). The topotactic decomposition of $NH_4(NiMoO_4)_2OH \cdot H_2O$ gives rise directly to $[NiMoO_4]_1$ layers extending along [010], similarly to what was observed with its Co analogue (31), and®-$NiMoO_4$ crystallizes at 455±C. Now that we have shown the structure of our HPA to be isostructural with the nickelotungstate (29), we know that in the Anderson-type $[NiH_6Mo_6O_{24}]^{4i}$ heteropolyanion, the $Ni(O_6)$ octahedron is linked by edges and surrounded by six octahedra containing Mo. Thus, its decomposition releases Þrst Mo and then Ni (in the presence of oxygens), so that the formation of®-$NiMoO_4$ microdomains occurs naturally after that of MoO_3 (P5, type II), and that ®-$NiMoO_4$ crystallizes after MoO_3 (Table 5). When dealing with the calcination of the HPA, MMo mixture, the formation of the Þnal coherent interfaces between ®-$NiMoO_4$ and MoO_3 depends on the relative rates of decomposition of the precursors. It seems that the conditions are better met by using precipitation or evaporation to dryness methods and that a type-I thermal behavior is even more favorable because of the lower crystallization temperature of MoO_3. When microcrystals of the latter are formed at low temperature, only nuclei of nickel molybdate can be supposed to exist at this stage. During the temperature increase, the still amorphous (or, at least, short-range ordered) domains of ®-$NiMoO_4$ have to nucleate in a cooperative way onto (and/or through) the thin sheets of recently crystallized MoO_3. A schematic illustration of the formation of ®-$NiMoO_4$ÐMoO$_3$ interfaces during calcination of type-I precursors is presented Fig. 6. The more numerous and the more disordered the crystallites, the more numerous and the more coherent can the interfaces be expected to be.

FIG. 6. Schematic illustration of the formation of ®-$NiMoO_4$ÐM interfaces during calcination of type I precursors. The rectangle repre a portion of space. (a) Just after crystallization of MoO_3 (280±C): cr lites of MoO_3 [1] inside a ÒcloudÓ of nuclei of nickel molybdate [After crystallization of ®-$NiMoO_4$ (450±C): crystallites of ®-NiMoO posited on MoO_3 [3], or interacting with MoO_3 [4], while some indiv MoO_3 [1] and ®-$NiMoO_4$ [2] crystals remain.

CONCLUSION

The catalytic results we have obtained show that, w MoO_3 is present beside $NiMoO_4$, the performance in oxidative dehydrogenation of propane is higher with $NiMoO_4$ than with ¯-$NiMoO_4$, in our conditions of re tion and with our methods of preparation. The main str tural difference between ® and ¯ forms consists of coordination of Mo, which is octahedral for ® and te hedral for ¯. Let us recall that the coordination of in orthorhombic MoO_3 itself is six or four depending whether the two long MoÐO bonds are taken into consi ation or not (54), so that an adaptation of Mo coordinat in MoO_3 appropriate to either case can be envisage can be assumed that the redox couple Mo^{6C}/Mo^{5C} ne sary for the oxidative dehydrogenation step of prop the value of which is different according to the ph (®-$NiMoO_4$, or MoO_3, or ¯-$NiMoO_4$), is better ada

to the reaction when domains of α-$NiMoO_4$–MoO_3 are present. The surface of an oxide or of an oxysalt is expected to be covered by oxygens in usual conditions; some of these oxygens are needed to activate the C–H bond of the alkane, and others ensure the dehydrogenation step by forming water accompanying the product, as in the present case of oxidative dehydrogenation (55). The mobility of the active and selective oxygens in Mo/Ni > 1 catalysts would thus be modified beneficially by the presence of α-$NiMoO_4$–MoO_3 domains. We have shown that the synergetic effects due to the low crystallographic misfits between two phases can be more or less strong according to the method of preparation. In the case of the [Ni–Mo–O] system, they are related to the relative rates of decomposition of the two components of the precursor, the ammonium metallomolybdate MMo and heteropolysalt HPA, which are responsible for the formation of α-$NiMoO_4$ in better contact with MoO_3.

ACKNOWLEDGMENTS

This work has been carried out within the frame of a GDR "propane" granted by Elf-Atochem and C.N.R.S. Thanks are due to B. Taouk (UTC) and M. Guelton (Université de Lille-I) for EPR experiments.

REFERENCES

1. Chaar, M. A., Patel, D., Kung, M. C., and Kung, H. H., *J. Catal.* **105**, 483 (1987).
2. Chaar, M. A., Patel, D., and Kung, H. H., *J. Catal.* **109**, 463 (1988).
3. Siew Hew Sam, D., Soenen, V., and Volta, J. C., *J. Catal.* **123**, 417 (1990).
4. Aguerro-Ruiz, A., Rodriguez-Ramos, I., Fierro, J. L. G., Soenen, V., Herrmann, J. M., and Volta, J. C., *Stud. Surf. Sci. Catal.* **72**, 203 (1992).
5. Mazzocchia, C., Aboumrad, C., Diagne, C., Tempesti, E., Herrmann, J.-M., and Thomas, G., *Catal. Lett.* **10**, 181 (1991).
6. Mazzocchia, C., Tempesti, E., and Aboumrad, C., Fr. Patent 89-00522 (1989).
7. Smits, R. H. H., Seshan, K., and Ross, J. R. H., *J. Chem. Soc., Chem. Commun.* **558** (1991).
8. Smits, R. H. H., Seshan, K., Leemreize, H., and Ross, J. R. H., *Catal. Today* **16**, 5l3 (1993).
9. Cavani, F., and Trifirò, F., *Catal. Today* **24**, 307 (1995).
10. Bettahar, M. M., Costentin, G., Savary, L., and J. C. Lavalley, J.-C., *Appl. Catal.* **145**, 1 (1996).
11. Ozkan, U., and Schrader, G. L., *J. Catal.* **95**, 137 (1985).
12. Ozkan, U., and Schrader, G. L., *Appl. Catal.* **23**, 327 (1986).
13. Ozkan, U., Gill, R. C., and Smith, M. R., *J. Catal.* **116**, 171 (1989).
14. Ozkan, U., Moctezuma, E., and Driscoll, S. A., *Appl. Catal.* **58**, 305 (1990).
15. Ozkan, U., Driscoll, S. A., Zhang, L., and Ault, K. L., *J. Catal.* **124**, 183 (1990).
16. Grzybowska, B., and Mazurkiewicz, A., *Bull. Acad. Pol. Sci., Sc. Chim.* **27**, 141, 149 (1979).
17. Alessandrino, G., Cairatti, L., Forzatti, P., Villa, P. L., and Trifirò, F., *J. Less Comm. Met.* **54**, 373 (1977).
18. Carbuciccio, M., and Trifirò, F., *J. Catal.* **45**, 77 (1976).
19. Forzatti, P., Lotzev, N., Gencheva, L., Pasquon, I., Shopov, D., and Villa, P. L., *J. Catal.* **65**, 369 (1980).
20. Nguyen, V. T., Tittarelli, P., and Villa, P. L., "Chem. Uses Molybdenum, Proc. Int. Conf. 3rd," p. 132 (1979).
21. Mazzocchia, C., Del Rosso, R., and Centola, P., *Rev. Portug. Quimica* **69**, 61 (1977).
22. Jung, S. J., Bordes, E., and Courtine, P., *in* "Proc. IXth Ibero-American Symp. on Catalysis, Lisbon, July 1984" (M. F. Portela, Ed.), p. 983.
23. Jung, S. J., Bordes, E., and Courtine, P., "Adsorption and Catalysis on Oxide Surfaces" (M. Che and G. C. Bond, Eds.), *Stud. Surf. Sci. Catal.* **21**, 345 (1985).
24. Wolfs, W. J., and van Hooff, J. H. C., "Preparation of Catalysts" (B. Delmon, P. A. Jacobs, and G. Poncelet, Eds.), p. 161, Elsevier, Amsterdam, 1976.
25. Courty, Ph., Marcilly, C., and Delmon, B., *Powder Technol.* **7**, 21 (1973).
26. Akimoto, M., and Echigoya, E., *J. Catal.* **29**, 189 (1973).
27. Ozkan, U., and Schrader, G. L., *J. Catal.* **95**, 120 (1985).
28. Nomiya, K., Takahashi, T., Shirai, T., and Muva, M., *Polyhedron* **6**, 213 (1987).
29. Eriks, K., Yannoni, N. F., Agarwala, U. C., Violet, E. S., and Baker, C. L., *Acta Cryst.* **130**, 1139 (1960).
30. Courtine, P., and Cord, P. Ph., *C.R. Acad. Sci. Paris* **270**, 946 (1970).
31. Cord, P. Ph., Thèse, Université Paris VI, Paris, 1972.
32. Cord, P. Ph., Courtine, P., Pannetier, G., and Guillermet, J., *Spectrochim. Acta. A* **28**, 1601 (1972).
33. Lates, A., Aissi, C. F., and Guelton, M., *J. Catal.* **119**, 368 (1989).
34. Lezla, O., Thèse, Université de Technologie de Compiègne, 1994.
35. Lezla, O., Bordes, E., Courtine, P., and Hecquet, G., "Europacat II, Maastricht, The Netherlands, Sept. 3–8, 1995," Abstract no. S3P8, p. 132.
36. Lezla, O., Bordes, E., and Courtine, P., "5th Europ. Conf. Solid State Chem., Montpellier, France, Sept. 4–7, 1995," Abstract no. A70, p. 164.
37. Belkouch, J., Monceaux, L., Bordes, E., and Courtine, P., *Mater. Res. Bull.* **30**, 149 (1995).
38. Belkouch, J., Taouk, B., Monceaux, L., Bordes, E., and Courtine, P., New Developments in Selective Oxidation II (V. Cortès-Corberan and S. Vic Bellon, Eds.), Elsevier, New York, 1994. [*Stud. Surf. Sci. Catal.* **82**, 819 (1994)]
39. Courtine, P., and Daumas, J. C., *C.R. Acad. Sci. Paris* **268**, 1568 (1969).
40. Mazzocchia, C., Del Rosso, R., and Centola, P., *J. Cal. Anal. Therm.* **11**, 3-12-1 (1980).
41. Merzouki, M., Taouk, B., Tessier, L., Bordes, E., and Courtine, P., *in* "Proc. Int. Congr. Catal., 10th, Budapest, 1992" (L. Guczi, F. Solymosi, and P. Tétényi, Eds.), p. 753, Akadémiai Kiadó, Budapest, 1993.
42. Tessier, L., Bordes, E., and Gubelmann-Bonneau, M., *Catal. Today* **24**, 335 (1995).
43. Ziółkowski, J., and Courtine, P., *Ann. Chim.* **8**, 303 (1973).
44. Chaze, A. M., and Courtine, P., *J. Chem. Res.* **1980** (S) 96, (M) 0954.
45. Callahan, J. L., Grasselli, R. K., Milberger, E. C., and Strecker, H. A., *Ind. Eng. Chem. Prod. Res. Develop.* **9**, 134 (1970).
46. Courtine, P., [A.C.S. Symposium Series] "Solid State Chemistry in Catalysis" (R. K. Grasselli and J. F. Brazdil, Eds.), Vol. 279, p. 37, Am. Chem. Soc., Washington, DC, 1985.
47. Ponceblanc, H., Millet, J.-M.M., Coudurier, G., Herrmann, J.-M., and Védrine, J. C., *J. Catal.* **142**, 373 (1993).
48. Courtine, P., and Véjux, A., *J. Solid State Chem.* **23**, 93 (1978). [**63**, 179 (1986)]
49. Véjux, A., Bordes, E., and Courtine, P., *Mat. Sci. Forum* **25/26** (1988).
50. Papachryssanthou, J., Bordes, E., Courtine, P., Marchand, R., and Tournoux, M., *Catal. Today* **1**, 219 (1987).
51. Bordes, E., and Courtine, P., *J. Catal.* **57**, 236 (1979).
52. Vedrine, J. C. (Ed.), Eurocat oxide, *Catal. Today* **20** (1994).
53. Hyde, B. G., and Bursill, L. A., *in* "The Chemistry of Non-Extended Defects in Non-Metallic Solids" (L. Eyring and M. O'Keeffe, Eds.), p. 347, North-Holland, Amsterdam, 1970.
54. Kepert, L. D., *in* "The Early Transition Metals," p. 62, Academic Press, New York, 1972.
55. Bordes, E., *in* "Elementary Reaction Steps in Heterogeneous Catalysis" (R. W. Joyner and R. A. van Santen, Eds.), p. 137, Kluwer Academic, New York, 1993.